



CHORUS

This is the accepted manuscript made available via CHORUS. The article has been published as:

Local spectroscopies across the superconductor-insulator transition

Hasan Khan and Nandini Trivedi

Phys. Rev. B **99**, 144516 — Published 17 April 2019

DOI: [10.1103/PhysRevB.99.144516](https://doi.org/10.1103/PhysRevB.99.144516)

Local spectroscopies across the superconductor-insulator transition

Hasan Khan^{1*} and Nandini Trivedi¹

(1) *Department of Physics, The Ohio State University, Columbus, OH 43210, USA*

(Dated: April 2, 2019)

We explore the manifestation of quantum fluctuations across the superconductor-insulator transition (SIT) in three different local measurements: the two-particle density of states $P(\mathbf{r}, \omega)$, compressibility $\kappa(\mathbf{r})$, and diamagnetic susceptibility $\chi(\mathbf{r})$ revealed through their local maps. The map of $\chi(\mathbf{r})$ displays growing fluctuations upon increasing temperature as well as upon tuning the quantum tuning parameter g , as expected, but remarkably, these fluctuations persist well below T_c as the SIT is approached, indicating the quantum nature of these fluctuations. The map of $\kappa(\mathbf{r})$ paints a similar picture when tuned via g , but in contrast to $\chi(\mathbf{r})$, we find a fundamental difference in its evolution with temperature, providing a complementary local probe to $\chi(\mathbf{r})$. $P(\mathbf{r}, \omega)$, obtained using Maximum Entropy analytic continuation of Monte Carlo simulations on 2D quantum Josephson junction arrays, shows strongly diminished zero-energy spectral weight in nearly-insulating islands, correlating with regions of suppressed $\kappa(\mathbf{r})$. We discuss the experimental implications of our results for scanning Josephson spectroscopy, compressibility, and scanning SQUID measurements, the first time these quantities have been discussed together in the context of quantum fluctuations.

I. INTRODUCTION

Since its discovery, superconductivity has long been a rich environment for understanding the quantum nature of our universe. Superconductors themselves are macroscopic condensates of paired electrons that owe their coherence to quantum mechanics. It is no surprise then that superconductivity in disordered two-dimensional thin film materials has proven to be a rewarding playground for studying quantum phase transitions (QPTs).¹⁻⁸ These QPTs are driven by quantum fluctuations between two competing phases of matter at zero temperature tuned by a non-thermal parameter g .⁹

For the superconductor-insulator transition (SIT) in thin films, theory¹⁰⁻¹² and experiment¹³⁻¹⁶ have both shown that the single-particle gap in the superconductor persists into the insulator. While the local amplitude remains finite and the single-particle density of states shows a robust gap, the coherence peaks become diminished and global superconductivity is lost. This suggests that Cooper pairs do not break up in the insulator, and in fact superconductivity is destroyed by the loss of global phase coherence between pairs on different islands. The SIT, then, is predominantly driven by quantum phase fluctuations.

We therefore use a bosonic description of a thin film superconductor in terms of a Josephson junction array (JJA) of superconducting islands, the Hamiltonian of which is related to the quantum XY model.^{17,18,21} Here, amplitude fluctuations are ignored and we directly simulate the phase degrees of freedom using quantum Monte Carlo (QMC). This gives us access to quantum phase fluctuations, which have been experimentally observed in global measurements²²⁻²⁴ but have only recently been imaged locally using scanning SQUID techniques.²⁵

In this paper we calculate local two-particle quantities such as compressibility, two-particle local density of states (LDOS), and local diamagnetic susceptibility in

order to highlight their importance in observing local quantum fluctuations. Local spectroscopies have previously played an important role in identifying a variety of physical phenomena, including the use of scanning tunneling spectroscopy (STM) to map spatial inhomogeneities in high- T_c cuprates,²⁶⁻²⁸ local compressibility measurements to observe electron-hole puddles in graphene,²⁹ and a combination of STM and spin-polarized STM to detect a possible signature of Majorana fermions in ferromagnetic chains on a superconductor.³⁰ Here we make predictions for experimental measurements that can be performed using scanning Josephson spectroscopy (SJS)³¹ and compressibility probes, which can be used to visualize quantum phase fluctuations. Notably, this is the first time each of these techniques has been discussed together in the context of imaging quantum fluctuations. Much like how temperature fluctuations of the cosmic microwave background have given us much insight into the structure of the early universe, we hope that local imaging of quantum fluctuations motivated by our results can expand our knowledge of quantum criticality.

The number-phase uncertainty principle that is at the heart of the SIT is also emerging as a paradigmatic model in quantum information. The “quantum phase slip” qubit describes a state with a well-defined flux in which number fluctuations introduce phase slips. The dual “Cooper pair box” is a qubit with well defined number of Cooper pairs in which Josephson tunneling creates number fluctuations.³² We discuss below how the qubit evolves across the SIT and connect these concepts to our results on spectroscopies.

Previous work involving global measurements have shown that the SIT is driven by phase fluctuations and the formation of vortices destroys the superconducting behavior. While the details of the phase transition on a global scale have been studied, the inhomogeneous nature of the transition remains an open question. Our results fill that gap and we present the first visual representation

of quantum fluctuations using several techniques. While previous work has attempted to understand the nature of the SIT, our work provides the first framework for imaging quantum fluctuations in the context of multiple spectroscopies: $\chi(\mathbf{r})$, $\kappa(\mathbf{r})$, and $P(\mathbf{r},\omega)$. We discuss several experimental probes that can be used to measure these spectroscopies and image local quantum fluctuations across the SIT.

Our specific results are as follows:

(1) The global two-particle DOS $P(\omega)$ is peaked at $\omega = 0$ in the superconducting phase due to the presence of a Cooper pair condensate. As the SIT is approached, this peak diminishes and the spectrum becomes gapped at the critical point, signaling a transition to a Cooper pair insulator. The global two-particle compressibility κ is also finite in the superconducting phase where Cooper pairs are free to tunnel and vanishes at the critical point where they become localized.

(2) The local compressibility $\kappa(\mathbf{r})$ in a disordered system captures the onset of quantum fluctuations as the SIT is approached. In the superconducting phase, increasing phase fluctuations create pockets of localized Cooper pairs where the compressibility is small. The LDOS $P(\mathbf{r},\omega)$ in these regions exhibits an $\omega = 0$ peak that is strongly suppressed whereas $P(\mathbf{r},\omega)$ outside of these pockets resembles the global $P(\omega)$ of a superconductor. As g is increased toward the SIT, fluctuations of $\kappa(\mathbf{r})$ increase mirroring the presence of increasing phase fluctuations. Interestingly, thermal fluctuations act to obfuscate the presence of these insulating pockets instead of increasing them in size. This provides an easy way to separate quantum fluctuations from thermal fluctuations in an experiment.

(3) The local diamagnetic susceptibility $\chi(\mathbf{r})$ also shows increasing fluctuations as the SIT is approached from the superconducting side. As a function of T/T_c , the standard deviation of $\chi(\mathbf{r})$ is peaked only in a narrow region around T_c for g deep in the superconducting phase. As g is increased toward the critical point, this peak broadens around T_c , indicating that fluctuations of $\chi(\mathbf{r})$ are appearing well-below T_c . The fact that these extra fluctuations exist far below T_c provide evidence that they are indeed of quantum origin.

II. MODEL AND METHODS

A useful model for understanding quantum fluctuations across the SIT is the 2D JJA model with Hamiltonian

$$\hat{H} = \frac{E_C}{2} \sum_i \hat{n}_i^2 - E_J \sum_{\langle ij \rangle} \cos(\hat{\theta}_i - \hat{\theta}_j) \quad (1)$$

where \hat{n}_i and $\hat{\theta}_i$ are canonically conjugate Cooper pair number and phase operators, respectively, that satisfy the commutation relation $[\hat{n}_i, \hat{\theta}_j] = i\delta_{ij}$. E_J links phases

on nearest neighbor sites via a Josephson coupling while E_C represents the charging energy of Cooper pairs on each site. When E_J is large, the phases align and the system is in a coherent superconducting phase. When the E_C term dominates, the system favors a well-defined number eigenstate, leading to quantum phase fluctuations that destroy the superconducting order and transition the system to a bosonic insulating phase. Thus we use the ratio $g = E_C/E_J$ as a knob to tune the system across a QPT between a superconductor and an insulator. It is important to emphasize that loss of global phase coherence is responsible for destroying superconductivity in our model. We assume that fluctuations of the superconducting amplitude are small and that we are working at temperatures well below the pair-breaking scale T^* of the superconducting island.

We simulate this model using QMC two different ways as shown schematically in Fig. 1a. In both cases we use a quantum-classical mapping to map the quantum JJA Hamiltonian to a classical action.^{17,18} First we map the 2D JJA to a (2+1)D XY model of classical phases, a language that is well suited for calculating the two-particle DOS $P(\omega)$ and compressibility κ . Simulations of the (2+1)D XY model are performed using a Wolff cluster algorithm³³ on system sizes 64×64 for global calculations and 24×24 for local calculations. To calculate diamagnetic susceptibility χ , we instead map the JJA to a (2+1)D integer current model (ICM) because the current basis is more natural for exploring the fluctuations of diamagnetic currents. We simulate the ICM using a worm algorithm³⁴ on a 64×64 lattice for both global and local calculations. See Supplementary I for more details on these mappings.^{19,20,35}

It is important to note that simulations calculating local quantities require a small amount of disorder to be introduced in order to create structure. Without disorder, local structure is washed out by Monte Carlo averaging. We introduce a small amount of disorder in the spatial bonds of each model by randomly removing a fraction $p = 0.1$ of Josephson couplings E_J throughout the lattice. This creates regions where insulating sites can nucleate and be detected by our local probes. There have previously been studies on disorder-tuned SITs,^{12,21} however we emphasize that the disorder in our model is static and the fluctuations we see are ultimately caused by tuning g , not disorder. It should be noted that while the presence of disorder does change the universality class of the transition,²¹ this change does not affect the qualitative relevance of our results. The Bose glass phase that emerges at weak disorder is negligible compared to the size of the superconducting and insulating regimes on the phase diagram.³⁶ We also note that while our microscopic model has only phase fluctuations, upon coarse-graining it contains both amplitude and phase fluctuations. The Higgs mode can be measured in our simulations via the dynamical conductivity.²¹ While the absorption threshold vanishes with increasing disorder, the spectral weight at finite energy remains.

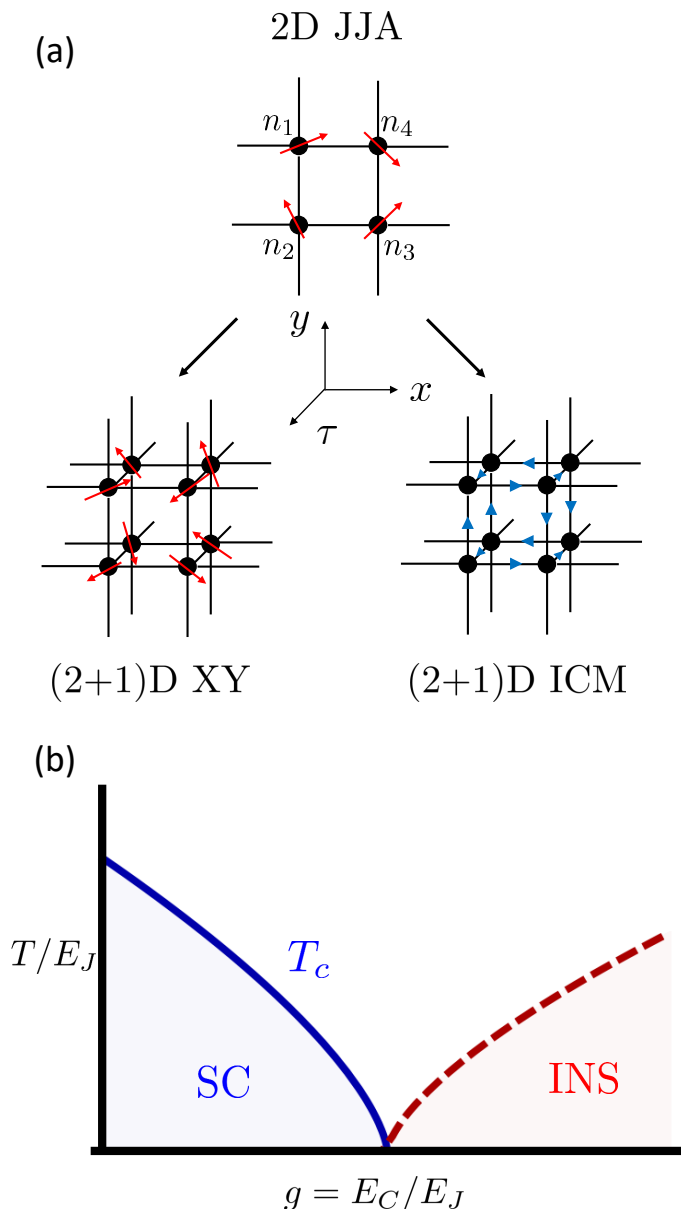


FIG. 1. Model and phase diagram. (a) We simulate the JJA Hamiltonian by mapping to two separate classical actions: XY and integer current model ICM. (b) Schematic phase diagram of the SIT along the g - T plane. At zero temperature, the JJA can be tuned through an SIT at $g = g_c$. At finite temperature, both the superconducting and insulating phases transition to normal states with increasing T . In-between there is a quantum critical regime.

Both the global $P(\omega)$ and local $P(\mathbf{r}, \omega)$ are calculated by analytically continuing imaginary time data to real frequencies using the Maximum Entropy Method (MEM).^{38,39} The procedure is delicate and we have performed extensive tests, including checking sum rules, to ensure the validity of our results (see Supplementary II for more information).³⁵

III. RESULTS

A. Bosonic spectral function

The bosonic Green's function in imaginary time is given by $G(\mathbf{r}, \mathbf{r}'; \tau) = \langle \hat{a}^\dagger(\mathbf{r}', \tau) \hat{a}(\mathbf{r}, 0) \rangle$ where \hat{a} , \hat{a}^\dagger are Cooper pair raising and lowering operators. In the language of the JJA we can rewrite³⁷ the raising operator in terms of its amplitude and phase as $\hat{a}^\dagger(\mathbf{r}, \tau) = \sqrt{\hat{n}(\mathbf{r}, \tau)} e^{i\hat{\theta}(\mathbf{r}, \tau)}$, but since we are ignoring on-site amplitude fluctuations we can write the Green's function purely in terms of the phase variable as

$$G(\mathbf{r}, \mathbf{r}'; \tau) = \langle e^{i(\hat{\theta}(\mathbf{r}', \tau) - \hat{\theta}(\mathbf{r}, 0))} \rangle \quad (2)$$

which is a spin-spin correlation function in the classical XY representation.

The real frequency spectral function $P(\mathbf{k}, \omega)$ is the imaginary part of the corresponding real frequency Green's function $G(\mathbf{k}, \omega)$

$$P(\mathbf{k}, \omega) = -\frac{1}{\pi} \text{Im} G(\mathbf{k}, \omega). \quad (3)$$

However, since we are working with imaginary time in our QMC, we need a way to analytically continue $G(\mathbf{k}, \tau)$ to a real frequency spectral function. This leads to the following relation between $G(\mathbf{k}, \tau)$ and $P(\mathbf{k}, \omega)$

$$G(\mathbf{k}, \tau) = \int_{-\infty}^{\infty} \frac{d\omega}{\pi} \frac{e^{-\tau\omega}}{1 - e^{-\beta\omega}} P(\mathbf{k}, \omega). \quad (4)$$

Solving this equation for $P(\mathbf{k}, \omega)$ amounts to inverting a Laplace transform. However, performing this procedure on QMC data of $G(\mathbf{k}, \tau)$ with error bars is non-trivial and requires the use of numerical analytic continuation techniques. In our work, we use MEM to obtain $P(\mathbf{k}, \omega)$ from $G(\mathbf{k}, \tau)$ and have validated our results by checking relevant sum rules.

We are particularly interested in the DOS which is the sum over momentum of the spectral function

$$P(\omega) = \sum_{\mathbf{k}} P(\mathbf{k}, \omega) = A(|\mathbf{r} - \mathbf{r}'| = 0, \omega) \quad (5)$$

This amounts to performing MEM on $G(|\mathbf{r} - \mathbf{r}'| = 0, \tau)$ data. In Fig. 2a we plot $P(\omega)/\omega$ as a function of g across the SIT. Since the form of (4) requires $A(-\omega) < 0$, we plot $P(\omega)/\omega$ to obtain a quantity that more closely resembles an experimentally measured DOS. We see that $P(\omega)/\omega$ is strongly peaked at $\omega = 0$ in the superconducting phase, corresponding to the existence of a Cooper pair condensate. As the SIT is approached, spectral weight shifts from the central peak to the finite energy modes on either side of ω until the system forms a gap for $g > g_c$. We plot the shift of this spectral weight from zero energy to finite energy modes in Fig. 2d. In Fig. 2c we plot the

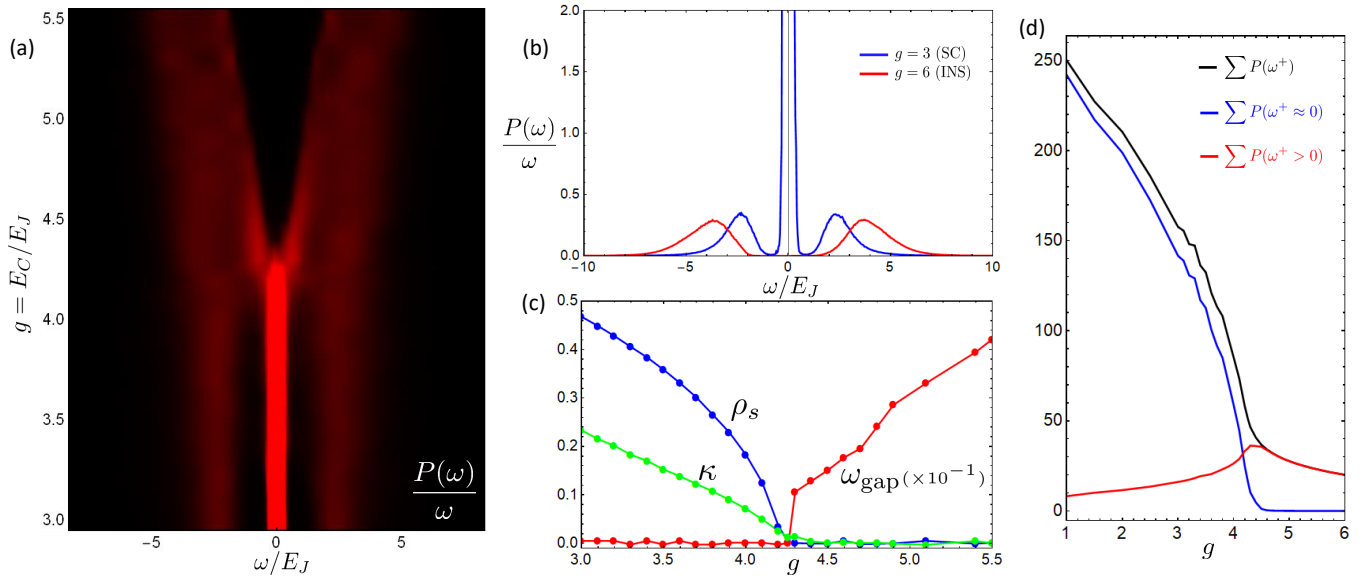


FIG. 2. Global DOS and energy scales across the SIT. (a) Global two-particle DOS $P(\omega)/\omega$ obtained from analytic continuation of the imaginary time Green's function $G(\tau)$ shown as a function of g . For $g < g_c \sim 4.26$ the DOS shows a zero energy peak corresponding to the Cooper pair condensate. As g increases, this weight shifts toward finite energy modes and for $g > g_c$ the system forms a gap characterized by the energy scale ω_{gap} , signaling the transition to an insulating state. (b) Cuts of $P(\omega)/\omega$ plotted for $g = 3$ (superconducting) and $g = 6$ (insulating) highlighting the difference in two-particle spectra between the two phases. (c) Energy scales near the SIT. The superfluid stiffness ρ_s and compressibility κ are finite in the superconducting phase but go soft at g_c . Similarly, on the insulating side, the two-particle gap scale ω_{gap} is finite and approaches zero as g_c is approached. Note that the error bars are the size of the data points here. (d) We show how the spectral weight in $P(\omega)$ shifts from $\omega = 0$ to finite energy modes with increasing g . At small g , most of the weight is centered around zero energy, however as g increases past the SIT this weight decreases to zero and increasingly shifts to finite energy states.

size of this gap ω_{gap} as a function of g along with other energy scales including the superfluid stiffness ρ_s and the compressibility κ (described in the next section). As we expect, ρ_s , κ , and ω_{gap} go soft at g_c from their respective sides of the transition.

B. Compressibility

The global compressibility κ is a quantity that characterizes fluctuations of the Cooper pair number density operator \hat{n} . We can define the average current along a generic spacetime bond b in the XY representation as

$$\langle j_b \rangle = -\frac{\partial \ln Z}{\partial A_b} = \langle K_b \sin(\partial_b \theta - A_b) \rangle \quad (6)$$

where $Z = \text{Tr} e^{-\beta \hat{H}}$ is the partition function, A_b is the element of an externally applied vector potential along bond b , and K_b is the coupling constant along that bond. We can then identify the average density $\langle n \rangle$ with the current along *temporal* bonds $\langle j_\tau \rangle$.¹⁷

The generalized electromagnetic response tensor

$$\Upsilon_{bb'} = \frac{\partial \langle j_b \rangle}{\partial A_{b'}} \quad (7)$$

describes the response of a current j_b along a spacetime bond b to an externally applied vector potential $A_{b'}$ along a bond b' . While the superfluid stiffness ρ_s can be obtained from the static, transverse long wavelength limit of the spatial response function Υ_{xx} , the compressibility is given by the static long wavelength limit of the temporal response function $\Upsilon_{\tau\tau}$ ⁴⁰

$$\Upsilon_{\tau\tau}(\mathbf{r}, \mathbf{r}'; \tau, \tau') = \frac{\partial \langle j_\tau(\mathbf{r}, \tau) \rangle}{\partial A_\tau(\mathbf{r}', \tau')} \quad (8)$$

$$= \langle -k_\tau(\mathbf{r}, \tau) \rangle \delta(\mathbf{r}, \tau) - \Lambda_{\tau\tau}(\mathbf{r}, \tau) \quad (9)$$

where $\langle -k_\tau(\mathbf{r}, \tau) \rangle = \langle K_\tau \cos(\partial_\tau \theta(\mathbf{r}, \tau)) \rangle$ and the temporal current-current correlator $\Lambda_{\tau\tau}(\mathbf{r}, \tau) = \langle K_\tau^2 \sin(\partial_\tau \theta(\mathbf{r}, \tau)) \sin(\partial_\tau \theta(0, 0)) \rangle$. Note that since we are performing linear response we take the limit $A_\tau \rightarrow 0$, and we make use of translational symmetry in the second line.

The compressibility κ is then the static, long wavelength limit of $\Upsilon_{\tau\tau}(\mathbf{r}, \tau)$

$$\kappa = \lim_{\mathbf{k} \rightarrow 0} \Upsilon_{\tau\tau}(\mathbf{k}, i\omega_n = 0). \quad (10)$$

Note that this amounts to calculating the response of the pair number density $\langle n \rangle \sim \langle j_\tau \rangle$ with respect to an externally applied electric potential $\phi \sim A_\tau$, which is the usual definition of compressibility.

In Fig. 2c we show κ as a function of g . κ is finite in the superconducting phase where Cooper pairs are phase coherent and are able to tunnel across the system. κ decreases as g_c is approached and vanishes in the Mott insulating phase where Cooper pairs become localized by phase fluctuations.

C. Local quantities

We next turn our attention to calculations of the LDOS $P(\mathbf{r}, \omega)$ and local compressibility $\kappa(\mathbf{r})$. $P(\mathbf{r}, \omega)$ is related to the local Green's function (2) at $\mathbf{r} = \mathbf{r}'$ by inverting (4) once again

$$G(\mathbf{r}, \tau) = \int_{-\infty}^{\infty} \frac{d\omega}{\pi} \frac{e^{-\tau\omega}}{1 - e^{-\beta\omega}} P(\mathbf{r}, \omega). \quad (11)$$

The local compressibility $\kappa(\mathbf{r})$ is given by the local response function $\Upsilon_{\tau\tau}(\mathbf{r}, \tau)$ in (9)

$$\kappa(\mathbf{r}) = \Upsilon_{\tau\tau}(\mathbf{r}, i\omega_n = 0) = \lim_{A_\tau \rightarrow 0} \frac{1}{\beta} \sum_{\mathbf{r}', \tau, \tau'} \frac{\partial j_\tau(\mathbf{r}, \tau)}{\partial A_\tau(\mathbf{r}', \tau')} \quad (12)$$

$$= \frac{1}{\beta} \sum_{\mathbf{r}', \tau, \tau'} (\langle -k_\tau(\mathbf{r}, \tau) \rangle \delta(\mathbf{r}', \tau') - \Lambda_{\tau\tau}(\mathbf{r}, \mathbf{r}', \tau, \tau')). \quad (13)$$

In order to extract local structure from our QMC simulations, we break translational symmetry by introducing a small fraction of bond disorder. In Fig. 3a we show a local map of $\kappa(\mathbf{r})$ at $g = 3.6$, near the SIT. We see that the system forms puddles where $\kappa(\mathbf{r})$ is significantly suppressed. These incompressible regions are locations where a large density of bonds have been cut, resulting in the formation of insulating islands. In Fig. 3b we plot the corresponding $P(\mathbf{r}, \omega)$ in two representative regions. We see a strong spatial correlation between the strength of $\kappa(\mathbf{r})$ and the distribution of low-energy spectral weight. The superconducting region highlighted in blue is highly compressible and has most of its spectral weight peaked strongly around $\omega = 0$, reflecting the strength of the superconducting condensate. The behavior of $P(\mathbf{r}, \omega)$ in this region matches that of the global $P(\omega)$ shown in purple, which reflects that of a globally phase-coherent superconductor. On the other hand, in the region highlighted in red with small compressibility, we see that the $\omega = 0$ peak in $P(\mathbf{r}, \omega)$ is highly suppressed. Here we can see evidence of a two-particle gap beginning to form as spectral weight shifts from $\omega = 0$ to finite energy modes, indicative of an emerging Cooper pair insulator.

It is important to emphasize that the emergence of insulating islands shown in Fig. 3a is caused by quantum phase fluctuations due to proximity to a quantum critical point. To illustrate this, in Fig. 4a we also plot $\kappa(\mathbf{r})$ as a function of g and temperature T . As g increases toward the SIT, fluctuations in $\kappa(\mathbf{r})$ increase, leading to

an increase in the size and prevalence of incompressible islands. Interestingly, as T increases the fluctuations in $\kappa(\mathbf{r})$ become smoothed out and the insulating islands become smaller. This is due to the fact that κ is sensitive specifically to number fluctuations. While quantum number fluctuations are expected to decrease as g increases, *thermal* number fluctuations increase as T increases due to higher energy number states becoming available. This is clearly seen in Fig. 4b, where the distribution of $\kappa(\mathbf{r})$ broadens significantly with increasing g , but narrows slightly with increasing T . This difference in behavior as $\kappa(\mathbf{r})$ evolves with g and T provides a way to distinguish quantum fluctuations from thermal fluctuations. We propose that an experiment that measures $\kappa(\mathbf{r})$ across the SIT will be able to directly image the presence of quantum fluctuations. The fact that these fluctuations are in fact *quantum* phase fluctuations is further confirmed by our results on the diamagnetic susceptibility.

D. Diamagnetic susceptibility

Phase fluctuations increase both as a function of temperature and a function of g . The question becomes how to separate thermal phase fluctuations from quantum phase fluctuations. A well-known property of a superconductor is the fact that it generates diamagnetic supercurrents in the presence of a magnetic field. In general the magnetization generated by an external field is related to the free energy by

$$\langle M \rangle = \frac{\partial(T \log Z)}{\partial B} \quad (14)$$

where $-T \log Z$ is the free energy in terms of the partition function Z and B is an external applied magnetic field. We can calculate the corresponding local diamagnetic susceptibility $\chi(\mathbf{r})$, which is sensitive to phase fluctuations, from linear response using a Kubo formula

$$\chi(\mathbf{r}) = -\frac{\partial \langle M(\mathbf{r}) \rangle}{\partial B} = \langle M(\mathbf{r}) M \rangle. \quad (15)$$

The local diamagnetic susceptibility is the response of a *local* induced magnetization $M(\mathbf{r})$ to a *global* applied magnetic field B . This amounts to calculating the correlator between the local magnetization $M(\mathbf{r})$ and the global magnetization M . To obtain $\chi(\mathbf{r})$, we perform QMC simulations in the dual ICM representation of the quantum JJA model. This representation is more suited to calculating quantities involving the supercurrent since the QMC configurations themselves are given in terms of integer currents (see Supplementary IB).³⁵

In the language of the ICM, we can write the total magnetization, assuming a uniform B -field in the \hat{z} -direction, as

$$\langle M \rangle = \frac{1}{2\beta} \left\langle \sum_{\langle ij \rangle, \tau} (x_i y_j - x_j y_i) j_{ij}^\tau \right\rangle \quad (16)$$

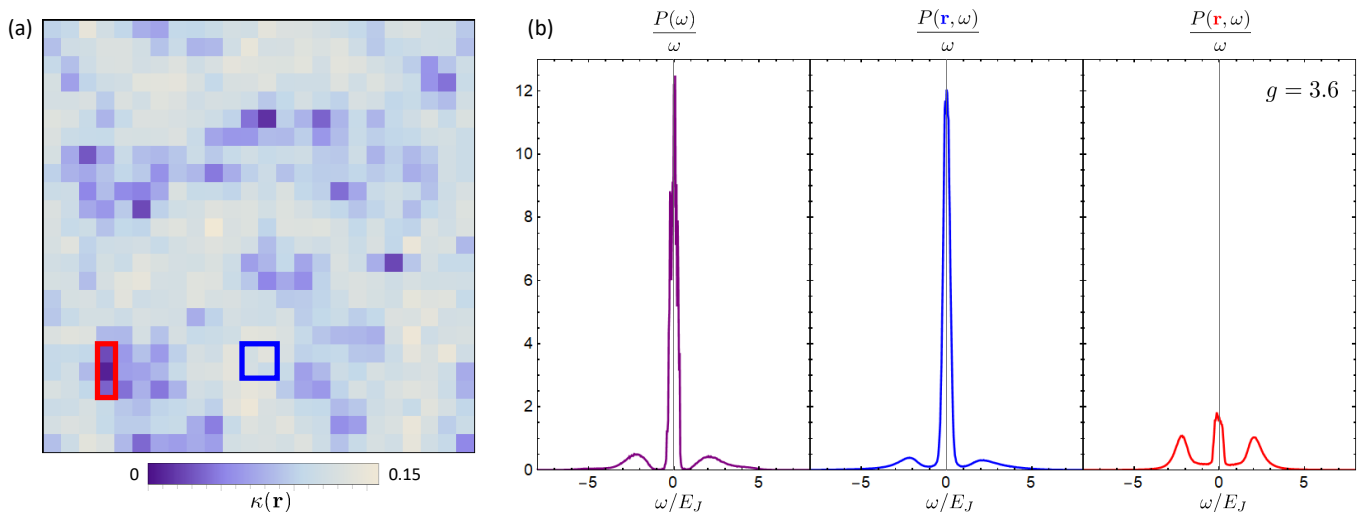


FIG. 3. Local compressibility and LDOS in a disordered system near the SIT. (a) Map of the local compressibility $\kappa(\mathbf{r})$ on a 24×24 lattice at $g = 3.6$, near the SIT. We introduce a small amount of bond disorder ($p = 0.1$) to produce local structure in our QMC data. We see that while the majority of system has finite κ (superconducting), the local $\kappa(\mathbf{r})$ map picks out large dark regions with κ near zero (insulating), as we would expect for a system exhibiting strong quantum fluctuations. This is reflected in the two-particle LDOS $P(\mathbf{r}, \omega)/\omega$ shown in (b). In the compressible region highlighted in blue, we see that $P(\mathbf{r}, \omega)/\omega$ has a peak at $\omega = 0$ characteristic of a superconductor. On the other hand, the incompressible region highlighted in red exhibits a peak that is highly suppressed at $\omega = 0$, indicating that this region is approaching an insulating regime. The global $A(\omega)/\omega$ is shown in purple for comparison.

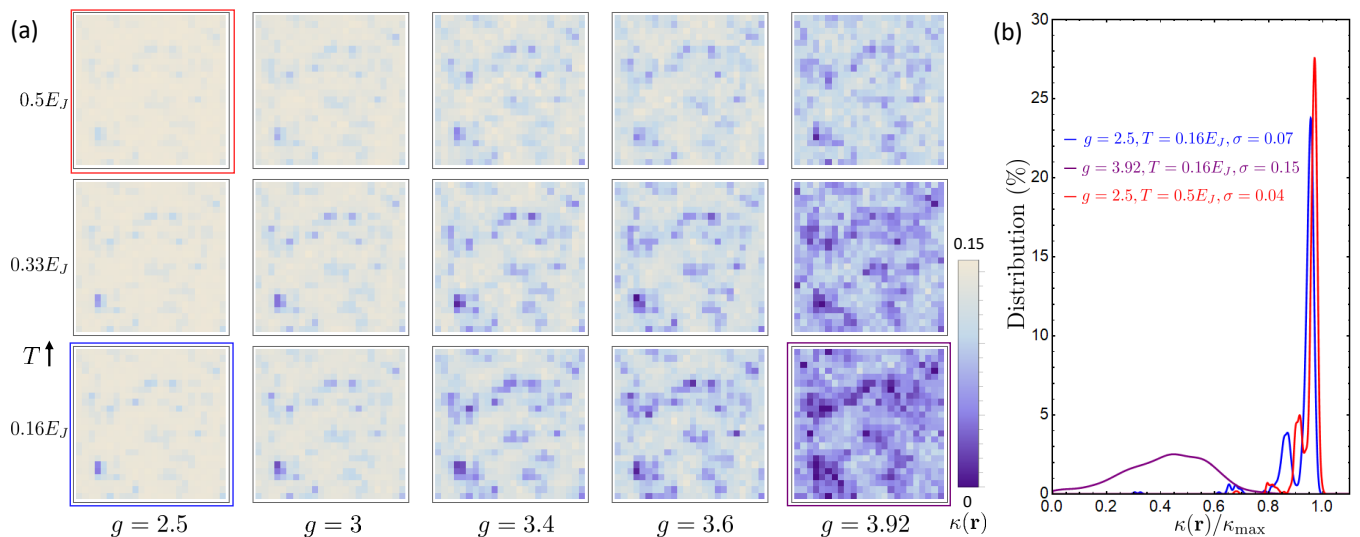


FIG. 4. Local compressibility maps and distributions. (a) Maps of the local compressibility $\kappa(\mathbf{r})$ on a 24×24 lattice as a function of g and temperature T on the superconducting side of the transition. We see that as the transition is approached with increasing g , fluctuations of the compressibility also increase. Interestingly, with increasing T we see that fluctuations in $\kappa(\mathbf{r})$ actually become smoothed out due to increasing number fluctuations. Since the behavior of $\kappa(\mathbf{r})$ as we evolve tuning g or T is different, we can separate the effects of thermal fluctuations from quantum fluctuations. (b) Distributions of $\kappa(\mathbf{r})$ for various maps. We see that as g increases for fixed T , the distribution of $\kappa(\mathbf{r})$ broadens significantly and the standard deviation σ increases. However, with increasing T and fixed g , the distribution only changes slightly and actually becomes narrower.

where j_{ij}^τ is an integer current on a spatial bond connecting sites i and j on timeslice τ . The spatial pattern that j_{ij}^τ is summed along comes from the corresponding vector potential of the uniform B -field, $\mathbf{A} = \frac{B}{2}(-x, y, 0)$. $M(\mathbf{r})$ is calculated from the discrete analog of the magnetiza-

tion current $\mathbf{j}(\mathbf{r}) = \Delta \times \mathbf{M}(\mathbf{r})$ where \mathbf{j} are the integer currents. Inverting this for $M_z(\mathbf{r}) = M(\mathbf{r})$ gives us

$$M(\mathbf{r}) = \int d\mathbf{r}' \cdot (\hat{z} \times \mathbf{j}(\mathbf{r}')). \quad (17)$$

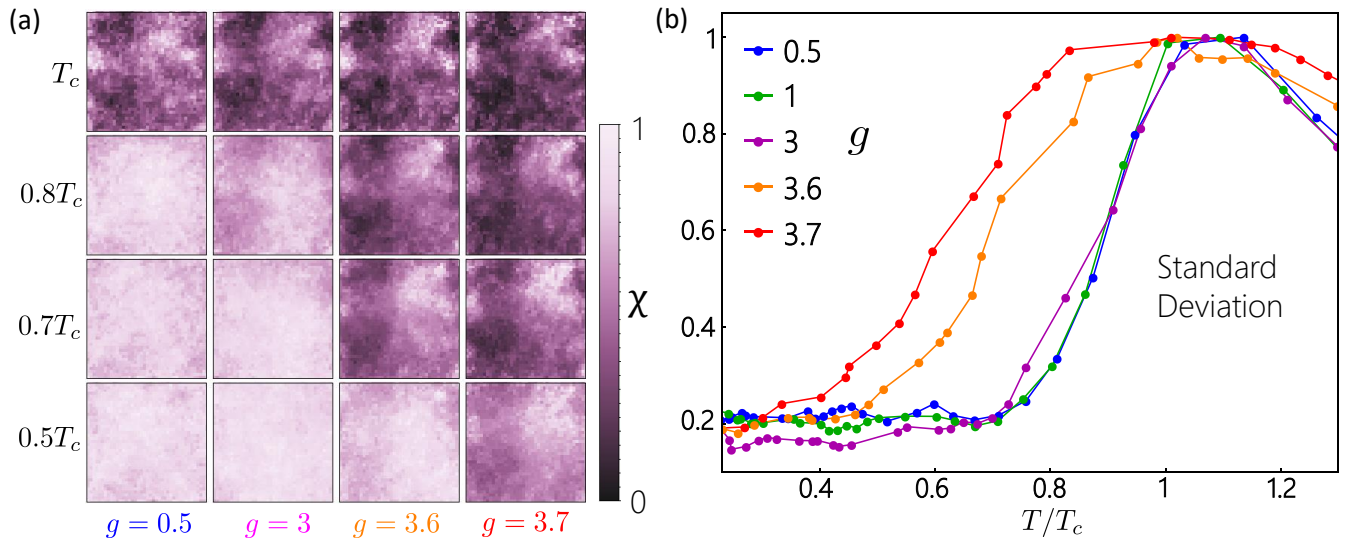


FIG. 5. Local diamagnetic susceptibility maps and standard deviation. (a) Local maps of the diamagnetic susceptibility $\chi(\mathbf{r})$ obtained on a 64×64 lattice as a function of g and T using the ICM representation. We see that for small g , $\chi(\mathbf{r})$ is large and uniform until the system approaches T_c , as expected of thermal fluctuations. However, as g is increased toward the SIT, fluctuations in $\chi(\mathbf{r})$ begin to appear well below T_c , suggesting that these additional fluctuations are quantum in nature. In (b) we plot the standard deviation of $\chi(\mathbf{r})$ for each value of g as a function of temperature. We see that while the standard deviation is always peaked around T_c , this peak broadens as the SIT is approached, pointing to the increasing importance of quantum phase fluctuations in this regime.

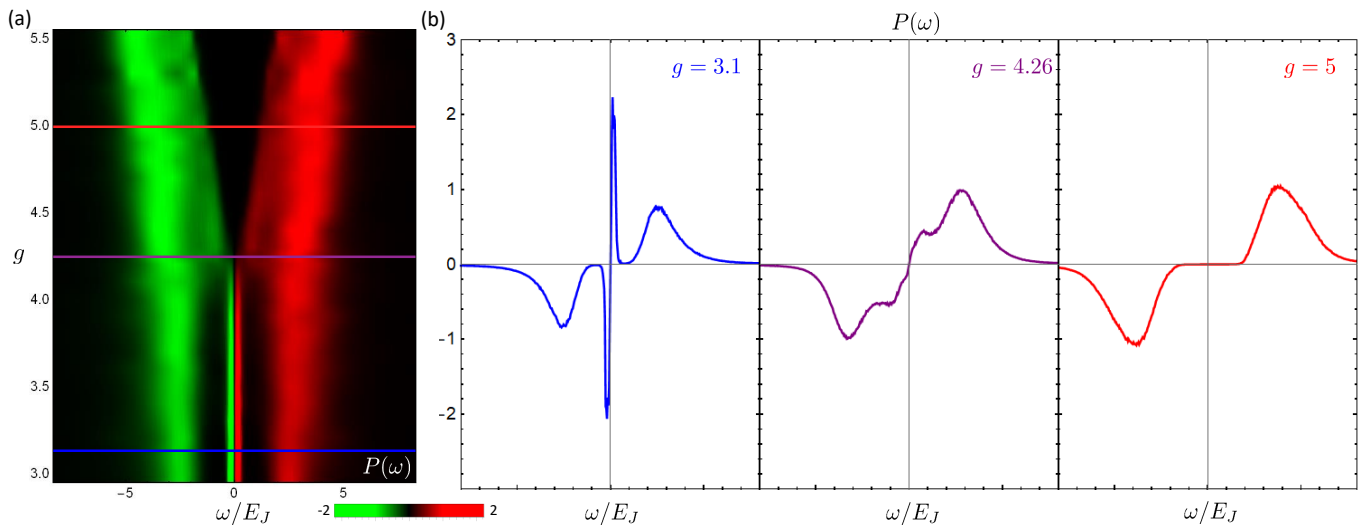


FIG. 6. DOS and qubits. (a) Evolution of the Cooper pair spectral function $P(\omega)$ across the SIT tuned by $g = E_c/E_J$, the ratio of charging energy to the Josephson energy. (b) The first cut shows a “Quantum phase slip” qubit whose behavior is consistent with a finite current at zero voltage, if we interpret the y-axis as the current and the x-axis as the voltage. In the second cut, we approach the transition described by a finite slope around $\omega = 0$, consistent with a finite resistance. The final cut describes a “Cooper pair box” qubit whose behavior is consistent with zero current until a critical voltage is reached.

In Fig. 5a we show local maps of $\chi(\mathbf{r})$ as a function of g and T/T_c . Here, T_c is the temperature at which the superconductor transitions to a normal state but still contains pairs; it should not be confused with the pair-breaking transition, that occurs at a much higher temperature. As expected, we observe that fluctuations of $\chi(\mathbf{r})$ increase with T/T_c due to thermal fluctuations. Simi-

larly, fluctuations of $\chi(\mathbf{r})$ also increase with increasing g . In both cases we see pockets with near-zero susceptibility beginning to form as phase fluctuations destroy the ability for coherent supercurrents to exist. However, interestingly, as g increases the fluctuations in $\chi(\mathbf{r})$ appear at lower values of T/T_c . The fact that fluctuations appear well below T_c when the system is near a quantum critical

point suggests that the fluctuations with increasing g are predominantly caused by *quantum* phase fluctuations.

This shows up as a broadening of the standard deviation of $\chi(\mathbf{r})$ across T/T_c as shown in Fig. 5b. For small g , the standard deviation is peaked mainly around T_c , suggesting that only thermal fluctuations are relevant in this regime. However as g increases the temperature range where standard deviation is large broadens to include temperatures well below T_c reflecting the importance of quantum fluctuations. This broadening of the temperature range of $\chi(\mathbf{r})$ fluctuations was recently observed in scanning SQUID experiments of the thin film superconductor NbTiN.²⁵ In the experiment, a scanning SQUID was used to directly image the local $\chi(\mathbf{r})$ and the corresponding standard deviation as a function of temperature and film thickness was found to qualitatively match that of theory. Importantly, this was the first time quantum fluctuations were directly imaged in an experiment.

IV. CONCLUSION AND OUTLOOK

For the first time, we have presented three different calculations of local two-particle response functions across the SIT: density of states $P(\mathbf{r}, \omega)$, compressibility $\kappa(\mathbf{r})$, and diamagnetic susceptibility $\chi(\mathbf{r})$. We have shown how these quantities can be used to probe the local structure of fluctuations across the SIT, which has been an open question until now. Particularly, for both $\chi(\mathbf{r})$ and $\kappa(\mathbf{r})$ we see an increase in local quantum fluctuations as the system approaches the critical point from the superconducting side, independent of thermal fluctuations

Our aim is to connect these calculations to spectroscopic measurements that can be performed in an experiment. We have already discussed how $\chi(\mathbf{r})$ can be measured using scanning SQUID techniques. We next turn our attention to measurements of $P(\omega)$ and $\kappa(\mathbf{r})$. It has previously been shown that it is possible capture the local structure of the superconducting order parameter using a combination of scanning tunneling spectroscopy (STM) and scanning Josephson spectroscopy (SJS) using a superconducting Pb tip.³¹ There, a suppression of the zero-energy peak measured in the SJS conductance was found on impurity sites, similar to our results on disorder sites of the JJA. We propose an experiment that uses SJS in conjunction with local compressibility measurements²⁹ to map out the evolution of quantum fluctuations across the SIT as we have done in Fig. 3 and 4. In particular, we expect a local compressibility measurement to be able to more cleanly separate quantum fluctuations from thermal fluctuations. In summary, we have made the first predictions for three quantities to be measured together in the context of imaging quantum fluctuations. We hope that these results will drive experimental interest in the visualization of quantum fluctuations and expand our understanding of quantum phase transitions.

We are also interested in connecting with recent developments in quantum information and quantum computing. As emphasized earlier, the essence of the SIT is the number-phase uncertainty principle. This can be used to define two types of dual qubits based on whether the phase dominates with quantum phase slips (QPS) disrupting that order (“QPS” qubit) on the SC site or whether the number of Cooper pairs is well-defined with Cooper pair tunneling disrupting the order (“Cooper pair box” qubit) on the insulating side.³² The behavior of the Cooper pair spectral function in Fig. 6 tracks the evolution of the qubit across the SIT.

QPS qubit: The QPS qubit is dominated by the inductive energy $E_J = \Phi_0^2/(2L)$, where L is the inductance of the loop and $\Phi_0 = h/(2e)$ is the SC flux quantum. The charging term mixes states with different fluxoid number $f = \Phi/\Phi_0$ where Φ is the flux through the loop and lifts the degeneracy at half-integer values of f . A current biased Josephson junction can be modeled as the dynamics of the phase in a slanted washboard potential. The phase is trapped in one of the minima yielding a zero voltage state, a superconductor, until the current exceeds a critical value.

Cooper pair box qubit: In the dual regime, the insulator has a fixed number of Cooper pairs on each island and is dominated by the charging scale $E_C = (2e)^2/(2C)$ where C is the capacitance of the island. Josephson tunneling mixes states with n and $n + 1$ Cooper pairs on an island and lifts the degeneracy at half integer values. In the voltage-biased configuration, charge is trapped in a potential minimum resulting in a zero current state, an insulator, for voltages below a critical value.

Once we understand how a qubit behaves in different regimes, it in fact becomes a device to measure and quantify the degree of fluctuations, both thermal and quantum, across QPTs. We expect these ideas will motivate developments in quantum measurement.

ACKNOWLEDGEMENTS

H.K. would like to acknowledge support from the Israel US bi-national foundation grant no. 2014325. N.T. acknowledges support from the DOE-BES grant DE-FG02-07ER46423. We would like to thank Yen Lee Loh for helpful discussions.

AUTHOR CONTRIBUTIONS

H.K. performed numerical calculations and data analysis. N.T. was responsible for project planning. Both authors contributed to discussion and manuscript preparation.

- ¹ Hebard, A. F. & Paalanen, M. A. Magnetic-field-tuned superconductor-insulator transition in two-dimensional films. *Phys. Rev. Lett.* **65**, 927 (1990).
- ² Shahar, D. & Ovadyahu, Z. Superconductivity near the mobility edge. *Phys. Rev. B* **46**, 10917 (1992).
- ³ Goldman, A. & Marković, N. Superconductor-insulator transitions in the two-dimensional limit. *Phys. Today* **51**, 39 (1998).
- ⁴ Adams, P. Field-induced spin mixing in ultrathin superconducting Al and Be films in high parallel magnetic fields. *Phys. Rev. Lett.* **92**, 067003 (2004).
- ⁵ Sambandamurthy, G., Engel, L. W., Johansson, A., & Shahar, D. Superconductivity-related insulating behavior. *Phys. Rev. Lett.* **92**, 107005 (2004).
- ⁶ Steiner, M. A., Boebinger, G., & Kapitulnik, A. Possible field-tuned superconductor-insulator transition in high-Tc superconductors: implications for pairing at high magnetic fields. *Phys. Rev. Lett.* **94**, 107008 (2005).
- ⁷ Stewart, M. D., Yin, A., Xu, J. M., & Valles, J. M. Superconducting pair correlations in an amorphous insulating nanohoneycomb film. *Science* **318**, 1273 (2007).
- ⁸ Gantmakher, V. F. & Dolgoplov, V. T. Superconductor-insulator quantum phase transition. *Physics-Uspexhi* **53**, 3 (2010).
- ⁹ Sachdev, S. *Quantum Phase Transitions* (Cambridge Univ. Press, Cambridge, 2011).
- ¹⁰ Ghosal, A., Randeria, M., & Trivedi, N. Role of spatial amplitude fluctuations in highly disordered s-wave superconductors. *Phys. Rev. Lett.* **81**, 3940 (1998).
- ¹¹ Ghosal, A., Randeria, M., & Trivedi, N. Inhomogeneous pairing in highly disordered s-wave superconductors. *Phys. Rev. B* **65**, 014501 (2001).
- ¹² Bouadim, K., Loh, Y. L., Randeria, M., & Trivedi, N. Single and two-particle energy gaps across the disorder-driven superconductor-insulator transition. *Nat. Phys.* **7**, 884 (2011).
- ¹³ Sacépé, B., Chapelier, C., Baturina, T. I., Vinokur, V. M., Baklanov, M. R., & Sanquer, M. Disorder-induced inhomogeneities of the superconducting state close to the superconductor-insulator transition. *Phys. Rev. Lett.* **101**, 157006, (2008).
- ¹⁴ Sacépé, B., Dubouchet, T., Chapelier, C., Sanquer, M., Ovadia, M., Shahar, D., Feigel'man, M., & Ioffe, L. Localization of preformed Cooper pairs in disordered superconductors. *Nat. Phys.* **7**, 239 (2011).
- ¹⁵ Mondal, M., Kamlapure, A., Chand, M., Saraswat, G., Kumar, S., Jesudasan, J., Benfatto, L., Tripathi, V., & Raychaudhuri, P. Phase fluctuations in a strongly disordered s-wave NbN superconductor close to the metal-insulator transition. *Phys. Rev. Lett.* **106**, 047001 (2011).
- ¹⁶ Sherman, D., Kopnov, G., Shahar, D., & Frydman, A. Measurement of a superconducting energy gap in a homogeneously amorphous insulator. *Phys. Rev. Lett.* **108**, 177006 (2012).
- ¹⁷ Wallin, M., Sørensen, E. S., Girvin, S. M., & Young, A. P. Superconductor-insulator transition in two-dimensional dirty boson systems. *Phys. Rev. B* **49**, 12115 (1994).
- ¹⁸ Sondhi, S. L., Girvin, S. M., Carini, J. P., & Shahar, D. Continuous quantum phase transitions. *Rev. Mod. Phys.* **69**, 315 (1997).
- ¹⁹ Suzuki, M. Quantum Monte Carlo methods—recent developments. *Physica A* **194**, 432 (1993).
- ²⁰ Villain, J. Theory of one- and two-dimensional magnets with an easy magnetization plane. II. The planar, classical, two-dimensional magnet. *J. Phys. France* **36**, 581 (1975).
- ²¹ Swanson, M., Loh, Y. L., Randeria, M., & Trivedi, N. Dynamical conductivity across the disorder-tuned superconductor-insulator transition. *Phys. Rev. X* **4**, 021007 (2014).
- ²² Crane, R. W. Armitage, N. P., Johansson, A., Sambandamurthy, G., Shahar, D., & Grüner, G. Fluctuations, dissipation, and nonuniversal superfluid jumps in two-dimensional superconductors. *Phys. Rev. B* **75**, 094506 (2007).
- ²³ Sherman, D., Pracht, U. S., Gorshunov, B., Poran, S., Jesudasan, J., Chand, M., Raychaudhuri, P., Swanson, M., Trivedi, N., Auerbach, A., Scheffler, M., Frydman, A., & Dressel, M. The Higgs mode in disordered superconductors close to a quantum phase transition. *Nat. Phys.* **11**, 188 (2015).
- ²⁴ Poran, S., Nguyen-Duc, T., Auerbach, A., Dupuis, N., Frydman, A., & Bourgeois, O. Quantum criticality at the superconductor-insulator transition revealed by specific heat measurements. *Nat. Comm.* **8**, 14464 (2017).
- ²⁵ Kremen, A., Khan, H., Loh, Y. L., Baturina, T. I., Trivedi, N., Frydman, A., & Kalisky, B. Imaging quantum fluctuations near criticality. *Nat. Phys.* **14**, 1205 (2018).
- ²⁶ Howald, C., Fournier, P. & Kapitulnik, A. Inherent inhomogeneities in tunneling spectra of Bi₂Sr₂CaCu₂O_{8-x} crystals in the superconducting state. *Phys. Rev. B* **64**, 100504(R) (2001).
- ²⁷ Pan, S. H. O'Neal, J. P., Badzey, R. L., Chamon, C., Ding H., Engelbrecht, J. R., Wang, Z., Eisaki, H., Uchida, S., Gupta, A. K., Ng, K.-W., Hudson, E. W., Lang, K. M., & Davis, J. C. Microscopic electronic inhomogeneity in the high-Tc superconductor Bi₂Sr₂CaCu₂O_{8+x}. *Nature* **413**, 282 (2001).
- ²⁸ Lang, K. M. Madhavan, V., Hoffman, J. E., Hudson, E. W., Eisaki, H., Uchida, S., & Davis, J. C. Imaging the granular structure of high-Tc superconductivity in underdoped Bi₂Sr₂CaCu₂O_{8+δ}. *Nature* **415**, 412 (2002).
- ²⁹ Martin, J., Akerman, N., Ulbricht, G., Lohmann, T., Smet, J. H., Klitzing, K. von, & Yacoby, A. Observation of electron-hole puddles in graphene using a scanning single-electron transistor. *Nat. Phys.* **4**, 144 (2008).
- ³⁰ Nadj-Perge, S., Drozdov, I. K., Li J., Chen, H., Jeon, S., Seo, J., MacDonald, A. H., Bernevig, B. A., & Yazdani, A. Observation of Majorana fermions in ferromagnetic atomic chains on a superconductor. *Science* **346**, 602 (2014).
- ³¹ Randeria, M. T., Feldman, B. E., Drozdov, I. K. & Yazdani, A. Scanning Josephson spectroscopy on the atomic scale. *Phys. Rev. B*, 161115(R) (2016).
- ³² Mooij, J. E., & Nazarov, Yu. V. Superconducting nanowires as quantum phase-slip junctions. *Nat. Phys.* **2**, 169 (2006).
- ³³ Wolff, U. Collective Monte Carlo updating for spin systems. *Phys. Rev. Lett.* **62**, 361 (1989).
- ³⁴ Prokof'ev, N. & Svistunov, B. Worm algorithms for classical statistical models. *Phys. Rev. Lett.* **87**, 160601 (2001).
- ³⁵ See Supplementary Material at [URL will be inserted by publisher] for details on the quantum-classical mapping

and analytic continuation using the Maximum Entropy Method.

- ³⁶ Gurarie, V., Pollet, L., Prokof'ev, N.V., Svistunov, B.V., & Troyer, M. Phase diagram of the disordered Bose-Hubbard model. *Phys. Rev. B* **80**, 214519 (2009).
- ³⁷ Fisher, M. P. A., Weichman, P. B., Grinstein, G., & Fisher, D. S. Boson localization and the superfluid-insulator transition. *Phys. Rev. B* **40**, 546 (1989).
- ³⁸ Gubernatis, J. E., Jarrell, M., Silver, R. N., & Sivia, D. S. Quantum Monte Carlo simulations and maximum entropy: dynamics from imaginary-time data. *Phys. Rev. B* **44**, 6011 (1991).
- ³⁹ Sandvik, A. W. Stochastic method for analytic continuation of quantum Monte Carlo data. *Phys. Rev. B* **57**, 10287 (1998).
- ⁴⁰ Kubo, R. Toda, M. & Hashitsume, N. *Statistical Physics II: Nonequilibrium Statistical Mechanics* (Springer, 2003).